9th International Symposium on Olfaction and Electronic Nose, ISOEN'02, Rome, Italy, 2002.

Chemical Detection Using Illumina's BeadArray ™ Technology

Bruce Forood, Theo Kotseroglou, Lori Clark, Michal Lebl, Minh-Ha Lieu, Bahram Kermani, David Barker, Todd Dickinson

Illumina, Inc, 9885 Towne Center Drive
San Diego, CA 92121, USA
bforood@illumina.com

Abstract

In this paper we describe our optically-based chemical detection system based on Illumina's BeadArray™ Technology [1,2,3]. In this approach, unique bead sensors are fabricated by either adsorbing or covalently attaching fluorescent solvatochromic dye molecules to the microsphere matrix. The responses are generated by measuring intensity changes, spectral shift, and time-dependent variations associated with the fluorescent sensors. Analysis of the intensity variations at a particular bandwidth during an image sequence generates a unique temporal response pattern for each chemical based on changes in microenvironment of the sensor. Pattern recognition software is then used to correlate the response pattern with the chemical being detected.

Keywords

BeadArray™ Technology, Solvatochromic, Optically-based chemical detection, Combinatorial chemistry, Electronic Nose.

INTRODUCTION

Illumina's chemical detection system uses cross-reactive optical sensor arrays based on Illumina's BeadArray™ platform.

Some of the unique characteristics of our optical chemical detection system include:

- Compatible with vapor (Optical Nose) as well as liquid (Optical Tongue) detection.
- Short sensor response times (milliseconds) for real-time detection.
- The ability to incorporate a large number of distinct sensors for improved selectivity.
- Inherent redundancy of individual sensors.
- Ease of sensor and array manufacturing.
- Fiber size and photonics components are ideal for miniaturization
- The sensors and the electronics can be physically separated to allow for the detection of flammable and/or toxic analytes

The main components of our system are

1- Sensor chemistry and fabrication
2- Instrumentation
3- Data analysis module

Sensor chemistry and fabrication

The bead array is assembled on an optical imaging fiber bundle consisting of about 50,000 individual fibers in a hexagonally packed matrix. The ends of the bundles are polished. Subsequently, one end is chemically etched, so that a well is produced in each of the 50,000 fibers. Then each well is loaded with a bead/sensor, which is approximately 5μm in diameter. This highly miniaturized array is about 1.5 mm total in diameter. The fiber-bundle separates the sample and the detection hardware and carries the fluorescence signal between them.

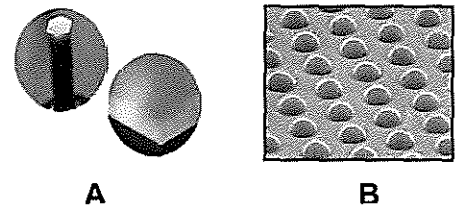

Figure 1. A) Optical imaging fiber bundle, B) Bead arrav.

Individual sensor types are prepared in batches using fluorescent solvatochromic compounds in conjunction with solid phase organic techniques, high throughput and combinatorial approaches.

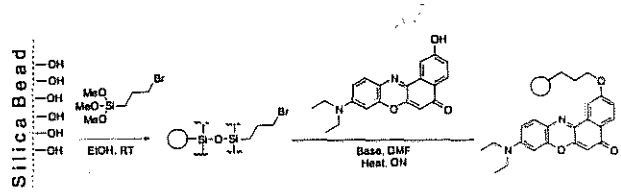

Figure 2. Attachment of Nile Red to microspheres via ether bond formation

High throughput approaches are particularly suitable for sensor development not only because selecting orthogonal sensors requires a large number of molecules, but also because of the need for repetitive and iterative cycles of synthesis and optimization [4]. Using this approach one can achieve selectivity, sensitivity and the desired stability for sensors.

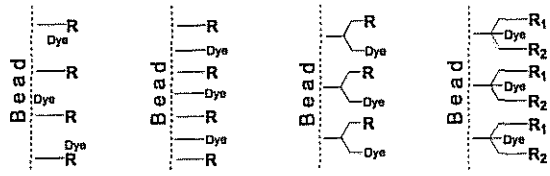

Figure 3. Various sensor formats

Sensors can be prepared either by adsorbing the dye of interest into the microsphere matrix or by covalently attaching the dye to the bead surface. One can then introduce a variety of functional groups on the bead surface to alter the bead characteristics and the microenvironment that an analyte will experience when coming in contact with the bead. Sensors responses to analytes of interest and their behavior (stability, sensitivity and selectivity) are routinely measured using our bench-top optical nose instruments.

Sensors are then pooled and loaded onto the fiber optics to generate the sensor array.

Instrument design and development

A basic diagram of the imaging system is shown in Figure 4. A white light source is used as the excitation source for benchtop instruments due to its flexibility in wavelength and power selection. For the portable instrument lasers and LEDs were explored. The excitation light is filtered before it excites the sensor. The resulting fluorescence of the sensors is transmitted back through the fiber, through either a bandpass or a tunable emission filter (Liquid Crystal Tunable Filter, LCTF) to the CCD camera where an image of the array is created. A series of these images is collected in time during an experiment allowing the fluorescence intensity of the sensors to be monitored during the interaction with the sample vapor.

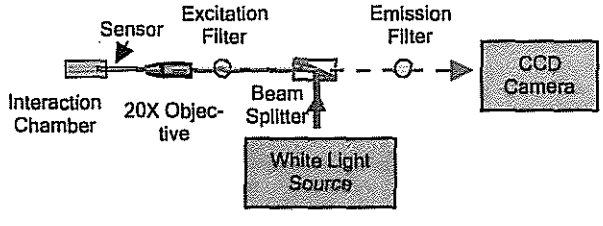

Figure 4. Basic diagram of the optical imaging system

As mentioned above, Illumina's optical nose is a flexible system that can be miniaturized for a variety of applications. Part of our effort has been focused on developing a handheld prototype in collaboration with ChevronTexaco for applications in the petroleum industry. Fig. 5 shows a picture of the portable handheld device. In this design the excitation source is a compact optically-pumped Nd:YVO_4 laser doubled in a KTP crystal. The sensors are directly excited (from the bead side) while the compact CCD captures the fluorescence emission photons that travel through the fiber bundle.

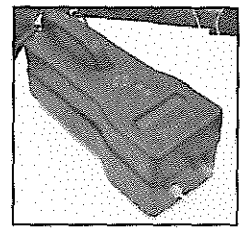

Figure 5. Portable handheld device

The vapor delivery system consists of a latching solenoid valve, a micro-pump and the interaction chamber where the sensor is situated. Teflon tubing and appropriate sample and purge gas (air) filters can be used.

Additional components such as LEDs for excitation and avalanche photodiode arrays for detection are currently under evaluation, with the goal of increasing sensitivity, compactness and reducing cost. Currently a laptop computer controls the electronics and acquires the data, which in turn are analyzed using Software written in LabVIEW and Matlab.

In addition to the bench top and handheld devices, we are also designing a miniaturized detection device with wireless capability that can transmit data to a central server. This device is planned for use in industrial process monitoring and homeland security in addition to other applications.

Data analysis module and informatics

The data collected from the CCD camera with purge gas or sample is a series of images, spaced in time. The image processing software locates the beads in each image, and follows their intensity values across the time sequence. From the time sequence of each bead, a series of features are extracted, using Principal Component Analysis (PCA) and Fuzzy Clustering (fig. 6). The resultant features and their corresponding class labels are then used in training a classifier system. The signals from unknown samples are passed through the trained classifier system, in order to obtain the appropriate class labels. We are also exploring more sophisticated analysis methods [5, 6] in order to increase the selectivity of the device and give us the ability to detect components of mixtures.

Proceedings of 8th World Multiconference on Systems, Cybernetics, and Informatics, vol. VI, pp. 148-149, Orlando, FL, 2004.

Optical Nose Signal Denoising and Detrending Using Wavelets

Bahram G. Kermani, Theo Kotseroglou, Behrouz Forood, David Barker, Michal Lebl

Illumina, Inc., 9885 Towne Centre Drive, San Diego, CA 92121, U.S.A.

ABSTRACT

Sensor miniaturization and the drive to develop ultra compact chemical sensing devices have received much attention in recent years. The characteristics, nature, and quality of signals are inevitably affected as sensors reduce in size. We have developed micron-size sensing elements using solvatochromic compounds and porous silica microspheres. Although many sensor elements, depending on their chemistry, show strong signals, a number of sensors demonstrate substantial drift and noise in their responses. The signals obtained from these miniaturized sensors comprise three dominant components: 1) the main component, corresponding to the response of the volatile of interest, 2) a piecewise linear trend, due to the delivery system and sensor recovery, and 3) a random noise component. While noise treatment can be done using many well-known methods, e.g., Fourier-based digital filtering, the treatment of the trend component is rather difficult. The objective of this study is to reduce the effect of the undesirable components of the time response, i.e., noise and trend, in the presence of weak signals. Trends are due to the non-stationary structure of the time-series signals, and the pulsatory switching of the volatiles in a nose system. Ad hoc methods of trend removal cause unsatisfactory results, by introducing severe discontinuities. In recent years, wavelet transform has become an invaluable tool for the treatment of non-stationary signals. In this study, the detrending and denoising is performed in one step, using wavelet transform. It is illustrated that for the optical-nose (O-Nose) signals, this method of preprocessing removes the original trend of the signals, while introducing no artificial aberrations.

Keywords: Wavelet Transform, Detrending, Denoising, Electronic Nose, Optical Nose.

INTRODUCTION

Illumina's chemical detection system uses optical sensor arrays based on Illumina's BeadArray™ platform [1-4]. The sensor array is assembled on an optical imaging fiber bundle. The ends of the bundles are polished. Subsequently, one end is chemically etched, so that a well is produced in each fiber. Then, each well is loaded with a bead/sensor, five microns in diameter. This highly miniaturized array is approximately 1.5 mm in total diameter. The fiber bundle separates the sample from the detection hardware, and carries the fluorescent signal between them. Individual sensor types are prepared in batches using fluorescent solvatochromic compounds in conjunction with solid-phase organic techniques, high-throughput and combinatorial approaches [5].

Depending on its chemistry, each bead can be considered as a single sensor, or a single member of a sensor family. Once exposed to an appropriate volatile, and excited with the appropriate light source, the sensor may fluoresce; and the fluorescence intensity and wavelength will change as a function of chemical environment. The fluorescent light is captured by a CCD camera, as a function of time.

Figure 1 illustrates a weak time-response, obtained from a single bead sensor exposed to a very low concentration of a certain volatile gas. The drift in the excitation light source is comparable in size to the amplitude of the signal. The abscissa represents the frame number. Each frame corresponds to one snapshot of the sensor signal on the CCD. The time separation between the frames is 100 msec. The ordinate represents the average of the pixel intensities in a 3x3 CCD grid, centered at the corresponding bead. This 3x3 grid is expected to contain more than 90 % of the energy contained in the bead intensity. At t=0, the sensor is exposed to the reference gas (nitrogen). At t=2.5 seconds (Frame 25), the sensor is exposed to the volatile gas of interest (herein referred to as the analyte), e.g., ethanol. At t=5 seconds (Frame 50), the analyte is removed and the sensor is, once again, exposed to the reference gas. The change of the gas from nitrogen to the analyte and back to nitrogen is responsible for the pulsatory shape of the time response. The exact location of the break-points (rise and fall of the pulse), however, is not exactly known, as the time lag of the solenoid valves, and the delay of the CCD data readout are not constant, i.e., they have stochastic deviations associated with them.

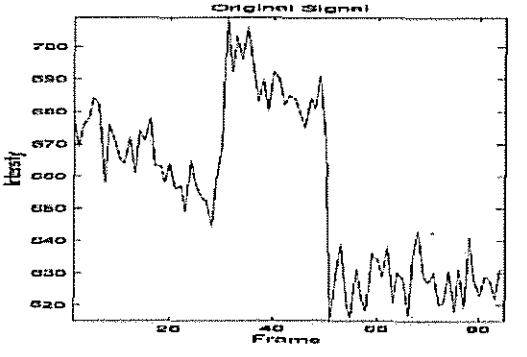

Figure 1: An exemplary weak time-response of a bead intensity.

METHODS

Figure 2-top shows the time response of four beads to four analytes. In addition to random noise, one common feature that is evident from these responses is the existence of a piecewise linear trend. The first and third patterns are referred to as positive responses, i.e., the exposure to the analyte of interest will give a higher count than the exposure to the reference gas. The fourth signal is referred to as a negative response. This means that the exposure to the analyte of interest will give a lower count than the exposure to the reference gas. The second pattern is considered zero response, i.e., it is indifferent to the exposure to the analyte of interest or the reference gas.

Using conventional methods, the removal of the piecewise linear trend proves not to be a trivial task to perform, as the exact location of the break points cannot be readily identified. For instance, one may consider the ad hoc method of finding the break points by placing a threshold on the intensities, fitting a line or cubic spline to those points, and subtracting the resultant curve from the original one. In addition to the challenge of finding an appropriate threshold value, such methods are highly undesirable as they are likely to introduce artificial discontinuities in the signal. As was mentioned earlier, the location of these break points cannot be specified a priori, as the lag in the switching of the gases and the delay in the CCD data readout are not deterministic. Regardless of the involved difficulties, detrending is necessary before further analysis.

In the field of signal processing, wavelet transform has proven to be an invaluable asset for the treatment of non-stationary signals [6-8]. One useful property of wavelets is having vanishing moments. A wavelet that has N vanishing moments can suppress the polynomials of degree N-1 and lower. A piecewise linear trend manifests itself as a piecewise first degree polynomial. Therefore, a suitable wavelet of order two or higher can, in theory, remove the linear trend.

Currently, a large library of wavelets is available. This library comprises the following wavelet families: Haar, Daubechies, Coiflets, Biorthogonal, Symlets, Meyer, Morlet, etc. Due to their linear phase, Biorthogonal wavelets are of high popularity in image and signal processing, and thus they were chosen in this study. The members of the Biorthogonal family include: 1.1, 1.3, 1.5, 2.2, 2.4, 2.6, 2.8, 3.1, 3.3, 3.5, 3.7, 3.9, 4.4, 5.5, and 6.8, where the first digit identifies the order of the reconstruction wavelet function, and the second digit indicates the order of the decomposition wavelet function. Of all the members of this family, Biorthogonal 2.2 was selected for this study, as it has the smallest support among the ones with at least two vanishing moments.

RESULTS

A 6-level decomposition was devised [9], as it was experimentally shown that with this composition, the Approximate component at Level 6 (A6), corresponds to the piecewise linear trend in the signal. The trend removal objective could thus be achieved by discarding the A6 components, followed by a signal reconstruction. However, since the objective was to also remove the noise, the Detail coefficients (Di, i=1..6) were thresholded using the Hard Threshold method [9], before reconstruction. The results of the complete denoising and detrending of the four signals of Figure 2-top are shown in Figure 2-bottom

The detrended signals are now suitable for the rest of the O-Nose processing. An example of such processing is ternary value assignment, i.e., labeling the responses as positive (Fig.2a,c), negative (Fig. 2d) or no-change (Fig. 2b). After applying the above detrending and denoising steps, this task becomes rather trivial.

CONCLUSION

In this study, it was demonstrated how wavelet analysis could be used for preprocessing the O-Nose signals. One prominent application of this preprocessing method is in the context of ternary label assignment to the O-Nose patterns. Lack of detrending and denoising can be detrimental for the task of ternary label assignment.

One drawback of the wavelet-based preprocessing is the number of CPU cycles it consumes. In traditional signal filtering using Fourier analysis, the coefficients of the filter are predefined. For every signal, a simple convolution operation with the filter coefficients renders the processed signal. The wavelet processing, in contrast, requires the step of decomposition and reconstruction for every signal, and thus is much more elaborate.

Biorthogonal wavelet of order 2.2 was selected for this study. This decision was made based on the linearity of phase, having a compact support, and being of order 2. This latter selection guarantees the suppression of polynomials of order 1 or lower. Since the trend was expected to be piecewise linear, suppression of the first degree polynomials was deemed sufficient.

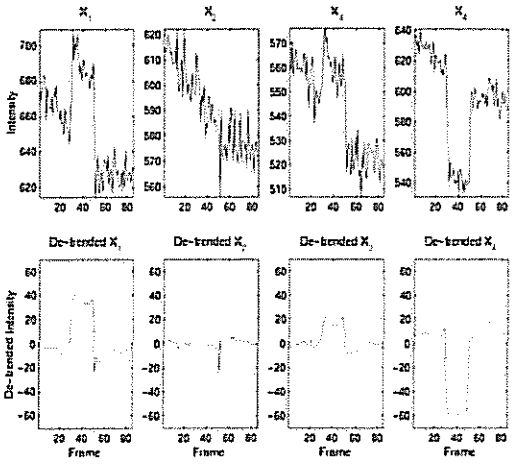

a b c d

Figure 2: Original signals (top) and detrended/denoised signals (bottom)

REFERENCES

[1] B. Forood, T. Kotseroglou, L. Clark, M. Lebl, M. Lieu, B. G. Kermani, D. Barker, T. Dickinson (2002) Chemical Detection using the Optical Nose System, **9th International Symposium on Olfaction and Electronic Nose**, ISOEN'02, Rome, Italy.

[2] T.A. Dickinson, K.L. Michael, J.S. Kauer, D.R. Walt (1999) **Anal Chem.**, pp.71, 2192.

[3] J. White, J.S. Kauer, T.A. Dickinson, D.R. Walt, (1996) **Anal Chem.**, pp.68, 2191.

[4] T.A. Dickinson, J. White, J.S. Kauer, D.R. Walt (1996) **Nature**, pp.382, 697.

[5] K.S. Lam, M. Lebl, V. Krchnak, (1997) **Chem. Rev.**, p.97, pp.411-448.

[6] S. Mallat (1998) A wavelet tour of signal processing, **Academic Press.**

[7] I. Daubechies, (1994) Ten Lectures on wavelets, **CBMS, SIAM**, 61, pp.271-280.

[8] Y. Meyer, S. Roques, Eds. (1993) Progress in wavelet analysis and applications, **Frotieres Ed.**

[9] M. Misiti, Y. Misiti, G. Oppenheim, J.M. Poggi (2000) MATLAB Wavelet Toolbox User's Guide, **Math Works, Inc.** Natick, MA.

B. G. Kermani, I. Fomenko, T. Kotseroglou, B. Forood, L. Clark
D. Barker, M. Lebl (2004) "Supervised Learning for Decoding
Beads in a Randomly-assembled Optical Nose,"

Computational Biology Workshop, Neural Information Processing Systems (NIPS)
Eighteenth Annual Conference, Whistler, B.C., Canada, 2004.

Decoding Beads in a Randomly-assembled Optical Nose

Bahram G. Kermani, Igor Fomenko, Theo Kotseroglou, Behrouz Forood, Lori Clark,
David Barker, Michal Lebl
Illumina, Inc. 9885 Towne Centre Drive, San Diego, CA 92122

Abstract

In Illumina technology, the term bead is synonymous with micro-sensors used in optical arrays. Unlike orderly arranged micro-arrays [1, 2], a randomly-assembled array would need to be processed via a so-called decoding step, in order to identify the location of each bead. In DNA-related applications, the decoding step is done via multi-stage hybridization to the complementary oligonucleotides (a.k.a., oligos) [3-6]. In the field of optical nose (O-Nose) sensors, since the probes are not oligo-based, this method would mandate adding the DNA-based probes to each sensor. This paper introduces an alternate method to DNA-based decoding. The sensors are decoded by exposing the mixture of the sensors to a certain analyte or to a series of pre-selected analytes. More specifically, the time-course of the exposure of the sensors to nitrogen followed by the exposure to the specific analyte is obtained. By selecting an appropriate analyte, one can obtain different signatures from the different optical sensors. This idea is the main focus of the following study. In the more complex cases, the signature of the sensors may not be completely resolvable by a single analyte. In this case, the methods developed by this study are still applicable. However, one would need to perform a series of exposures to multiple analytes. At each stage of the series, the same procedure is executed. After the final stage, the individual results are pooled together, in order to make a composite decision. The major assumption for enabling the above claim is that even though each analyte, by itself, cannot break the complexity of the mixture, the combination of the carefully selected analytes would enable

one to do so. The methods of this study are based on subspace classification.

Introduction

Most traditional electronic nose sensors are based on a small number of discrete sensors. Illumina's O-Nose technology is radically different from the electronic nose (E-Nose) technologies by several factors, e.g., the number of sensors. In an O-Nose application, one can easily obtain 2000 usable sensors. The quantity of sensors, however, does come at a price, i.e., the necessity for a decoding procedure. Upon assembly, the beads (sensors) are randomly distributed on the array substrate. The process by which one would identify the location of each bead is referred to as decoding. The decoding step plays a challenging role in the O-Nose technology. In this paper, a novel method of decoding randomly-assembled arrays is introduced. This is based on subspace classifier method [7].

An alternate method of decoding such a problem is based on unsupervised learning [8]. In this method, the time-course signal is first compressed, and then processed using a clustering algorithm, e.g., Fuzzy C-Means (FCM). In general, since the supervised learning method can make use of class labels, its performance is expected to be superior to that of the unsupervised learning.

Methods

A method of supervised learning was devised for this problem. More specifically, three sets of data were provided along with their corresponding class labels. A fourth set, which contained the combination of the three bead types, was also provided. For this latter set of beads, no class label was provided. The objective of this study was to

place labels (1, 2, or 3) on every bead of the fiber bundle containing the mixture of the three bead types. Figure 1 illustrates the prototype time-course of the three bead types under test, along with the name of the compounds that the sensors are made of [8].

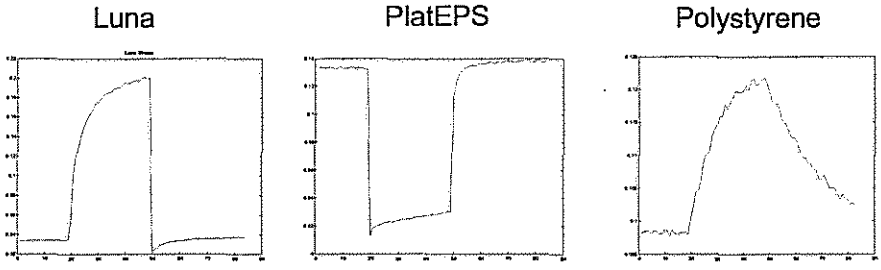

Figure 1: Class prototypes, i.e., the projections onto the first principal component of the class Luna (a), Plat-EPS (b), and Polystyrene (c). (Abscissa and ordinate represent the frame number (time) and bead intensity, respectively.)

Figure 2 shows the profile of 49 randomly selected bead-types from the multi-bead-type fiber bundle, i.e., the fiber bundle containing the mixture of the beads. It is notable that not all of the bead-types follow the above general patterns, to a great degree.

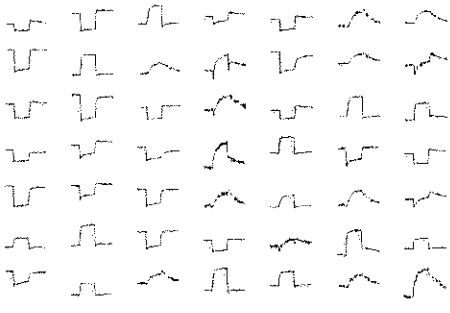

Figure 2: A sample of the three bead-type mixture. Each time trace represents one bead-type in the mixture.

For every bead-type, three features were extracted, one feature per class. These features were based on the normalized cross-correlation between the pattern of a bead-type and the class prototypes. The representation of the bead-type in this N-dimensional space (N=3) is projected into the N-2 = 1-dimensional subspaces. In each subspace, a negative label is assigned to the bead-type, if it falls on the negative side of the subspace. For instance, consider the projection into the subspace spanned by X3. In this case, if a bead-type's projection falls on the negative side of the X3 axis, the bead-type is labeled as "not belonging to Class 3." If the projection falls into the positive side, no label is assigned. This process is repeated for all the other possible subspaces. At the end of this process, the partial (negative) calls are combined, and a composite call is deduced. For example, if the bead-type does not belong to X3 and does not belong to X2, then by deduction it has to belong to UoD – {X2, X3} = X1, where UoD is the Universe of Discourse. Occasionally, a bead-type may not have enough negative calls to satisfy a unique deductive solution. In that case, the bead-type would receive a no-call label.

In an attempt to rank the quality of the decoded beads, a score was assigned to each decoded bead-type. This score was a function of the Mahalanobis distance of the bead to (the other members of) its assigned class. The raw Mahalanobis distances were processed via sigmoidal functions, in order to transform the distances to scores, bounded in [0,1]. The sigmoidal function was designed such that at Mahalanobis distances of 3 and 10, the scores were approximately 1 and 0, respectively. These numbers were selected based on the heuristic assumptions that for a normal distribution, a Z-distance of 3 contains more than 99% of the data, and data points with Z-distance of 10 or higher can be labeled as outliers [9].

Results

Figure 3 shows the 3-D representation of the individual bead-types, i.e., three fiber bundles, each containing only one bead type. Components of each dot (bead) on x, y, and z axes correspond to the projection of the bead time-response onto the first principal component of Class1, Class2 and Class3, respectively.

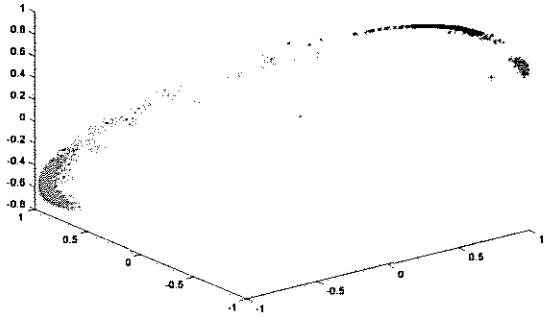

Figure 3: Bead labeling, based on training separate classes. Each symbol/shade represents one labeled class. X, Y, and Z axes represent the projection of the bead's time-response onto the first principal component of Classes 1, 2, and 3, respectively.

Figure 4 corresponds to the multi-bead bundle. This fiber bundle contains beads from all the three types. This is obvious from the span of the values.

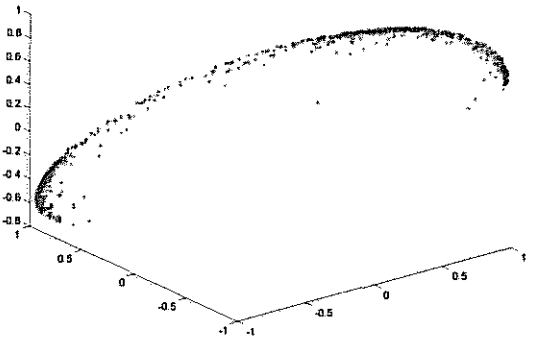

Figure 4: The multi-bead bundle projections. The plot represents the mixture of three bead-types. X, Y, and Z axes represent the projection of the bead's time-response onto the first principal component of Classes 1, 2, and 3, respectively.

Figure 5 shows the results of the multi-bead-type fiber bundle after decoding. The resemblance of this figure to Figure 3 provides a visual confirmation on the quality of the decoding. The classes, however, are not completely separated, i.e., there is no significant gap between the classes. This can be partially attributed to the fact that sensor responses are not always pure, i.e., they do not always belong to one of the three classes. Some sensors may fail to respond properly, as it is evident in Figure 2.

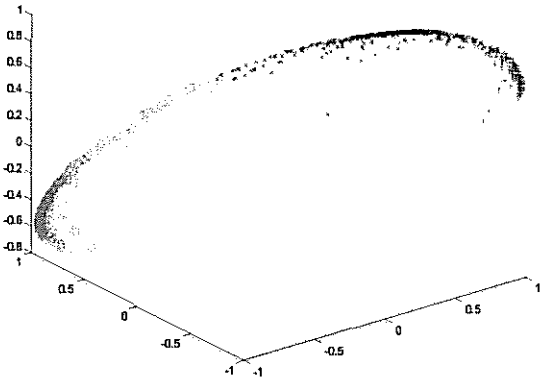

Figure 5: Bead labeling using supervised learning. X, Y, and Z axes represent the projection of the bead's time-response onto the first principal component of Classes 1, 2, and 3, respectively.

Figure 6 shows the beads of the three classes of the multi-bead fiber bundle, with scores greater than the arbitrary threshold of 0.7 (all shown in red). The rest of the beads are shown in green.

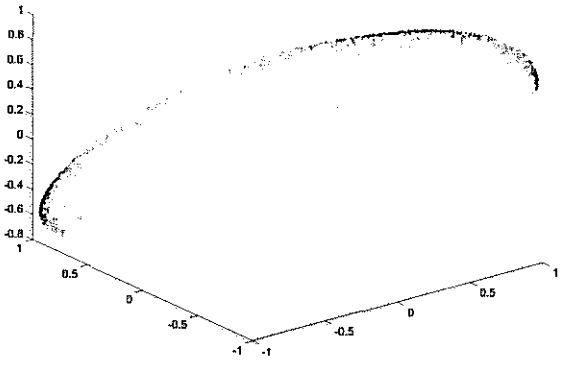

Figure 6: Points with score greater than 0.7. X, Y, and Z axes represent the projection of the bead's time-response onto the first principal component of Classes 1, 2, and 3, respectively.

Given the arbitrary threshold of 0.7 on the scores, one can bin the high-quality beads into three classes, as shown in Table 1.

Sensor	Total beads decoded	Acceptable beads
Luna	212	168
PlatEPS	557	453
Polystyrene	473	367
Total	1240	988

Table 1: The number of high-quality beads (score > 0.7) in different classes

According to Table 1, approximately 80% of the beads were decoded (988/1240 = 0.8) with Score > 0.70. The resultant decoded beads were visually confirmed for accuracy of the calls. The decode efficiency (DE) of 80% is to contrast with the 10 % DE achieved by an unsupervised learning method [8].

Conclusion

Supervised learning results in higher decoding efficiency (80 %) in the prediction of the unknown classes, as compared with an unsupervised learning method (which resulted in 10 % decoding efficiency). The supervised learning is also less sensitive to the number of elements in each class. In particular, it is less sensitive than the unsupervised learning to the imbalance in the number of items in clusters. This is mainly due to the fact that in supervised learning, one can exploit the domain-specific prior knowledge.

References

[1] M.J. Heller (2002) "DNA Microarray Technology: Devices, Systems, and Applications," *Annu Rev Biomed Eng* 4, 129-53.
[2] D. Shalon, S.J. Smith, P.O. Brown (1996) "A DNA microarray system for analyzing complex DNA samples using two-color fluorescent probe hybridization," *Genome Res.* 6(7): 639-45.

[3] T.A. Dickinson, K.L. Michael, J.S. Kauer, D.R. Walt (1999) *Anal Chem.*, pp.*71*, 2192.
[4] J. White, J.S. Kauer, T.A. Dickinson, D.R. Walt, (1996) *Anal Chem.*, pp.*68*, 2191.
[5] T.A. Dickinson, J. White, J.S. Kauer, D.R. Walt (1996) *Nature*, pp.*382*, 697.
[6] K.S. Lam, M. Lebl, V. Krchnak, (1997) *Chem. Rev.*, p.97, pp.411-448.
[7] J. Laaksonen (1997) "Local Subspace Classifier," *Proceedings of ICANN'97*, Stockholm, Sweden. pp. 37-40.
[8] B. Forood, T. Kotseroglou, L. Clark, M. Lebl, M. Lieu, B. G. Kermani, D. Barker, T. Dickinson (2002) Chemical Detection using the Optical Nose System, 9th International Symposium on Olfaction and Electronic Nose, *ISOEN'02*, Rome, Italy.
[9] MATLAB Statistics Toolbox, *Math Works, Inc.* Natick, MA.